Journal of Sound and Vibration (1997) **200**(1), 15–29

CUTTING STATE IDENTIFICATION

B. S. Berger, I. Minis, M. Rokni, M. Papadopoulos, K. Deng and A. Chavalli

Department of Mechanical Engineering, University of Maryland, College Park, MD 20742, *U.S.A.*

(*Received* 22 *November* 1995, *and in final form* 11 *July* 1996)

Cutting states associated with the orthogonal cutting of stiff cylinders are identified through an analysis of the singular values of a Toeplitz matrix of third order cumulants of acceleration measurements. The ratio of the two pairs of largest singular values is shown to differentiate between light cutting, medium cutting, pre-chatter and chatter states. Sequences of cutting experiments were performed in which either depth of cut or turning frequency was varied. Two sequences of experiments with variable turning frequency and five with variable depth of cut, 42 cutting experiments in all, provided a database for the calculation of third order cumulants. Ratios of singular values of cumulant matrices find application in the analysis and control of orthogonal cutting.

1. INTRODUCTION

The objective of constructing efficient machine tools capable of producing parts of high quality with minimum human intervention has motivated numerous research efforts directed towards the understanding of fundamental aspects of cutting dynamics. Although models of single point turning are available, identification of all of the relevant processes, their interdependence and mathematical representation is as yet an unresolved task of considerable difficulty. A review of cutting vibration research is given in reference [25].

Linear cutting models have been represented in the frequency domain by a single transfer function or a third order flexibility matrix, [10, 19, 15]. Structural transfer functions have been experimentally identified in references [24] and [9]. Models based on steady cutting which relate cutting forces to the shear angle are developed in reference [14]. The dynamic counterpart of this theory has been used to develop non-linear cutting force models [15, 27, 12]. Time series analysis has been used to estimate parameters in linear models which best approximate cutting measurements [18, 2]. These results have provided a basis for methods of chatter prediction. Linear prediction models characteristically represent the cutting system by a closed loop with time delays. Linear control theory has been applied to determine the critical depth of cut [19].

Recently developed signal processing methodologies including neural networks and wavelets have been applied to the analysis and control of cutting dynamics. In reference [23] two back propagation neural networks, one for frequency estimation, the other for sine wave identification, were trained on numerically generated sine and triangular waves. The choice of training functions was predicated on the assumption that ''regenerative self-excited vibrations and forced chatter created by force distributions amplified by structural resonance have a distinctive pattern''. These chatter vibrations were assumed to have a harmonic shape, exponential growth of amplitude and a frequency close to the lowest natural frequency of the structure. Tests were conducted on turning long slender bars. The trained neural network was able to detect the onset of the transition to chatter.

0022–460X/97/060015 + 15 $25.00/0/sv960666

No attempt was made to detect other cutting states. The cutting state to be identified was characterized by other means before numerically generated functions were constructed to train the neural network.

Wavelet transforms were employed in reference [8] to study the dynamical characteristics and frequency content of non-regenerative thread and slot cutting processes. Tool acceleration and cutting forces were measured for feeds parallel and perpendicular to the rotational axis of a turning specimen. The effects of spindle speed, feed rates and width of cut were studied. Time–frequency plots based on Gaussian wavelet transforms were used to detect and characterize non-stationary phenomena such as built-up edge breakage. Wavelet analysis suggested that the non-regenerative cutting process is probably quadratically non-linear [3]. Chaotic vibrations were detected for several sets of cutting parameters. It was suggested that a wavelet transform combined with a chatter model be used for on-line control of the cutting process. However, real time or simulated control was not reported. Differentiation between various cutting states was made on the basis of qualitative features of power spectra and wavelet based time frequency plots. Chaotic behavior was identified through the calculation of phase plane plots, power spectra, Poincaré maps and fractal dimensions [1].

The identification of cutting states, associated with the orthogonal cutting of stiff cylinders, is realized in the following through an analysis of the behavior of the singular values of a Toeplitz matrix of third order cumulants of acceleration measurements. A bispectral analysis of cutting tool acceleration measurements has shown [3] that the cutting process is quadratically phase coupled. The determination of coefficients in an autoregressive approximation of the bispectrum [20] involves the construction of an unsymmetric Toeplitz matrix, **R**, of third order cumulants. It is shown that the behavior of the dominant pairs of singular values of **R** provides a basis for the identification of cutting states. In particular, the ratio of the two pairs of largest singular values, the R-ratio, is shown to differentiate between light cutting, medium cutting, pre-chatter and chatter states. Sequences of cutting experiments were performed in which either depth of cut or turning frequency was varied while all other cutting parameters were held constant. Two sequences of experiments with variable turning frequency and five with variable depth of cut, a total of 42 cutting experiments, were studied. Results typical of the entire set are presented for a sequence of variable cutting depth and a sequence of variable turning frequency. The R-ratio evaluated at maxlag $= 100$, equation (4), is close to one for all cases of light cutting and two or greater for chatter. For intermediate states the ratio increases as the chatter state is approached.

A description of the experimental apparatus is followed by definitions and results from bispectral theory, third order recursion and the **R** matrix. Results from the theory of singular value decomposition are presented and applied to three different phase coupled trigonometric functions. R-ratios are computed as a function of lags, exhibiting similarities with R-ratios versus lags based on cutting acceleration measurements. An analysis of sequences of cutting experiments shows that singular values of the **R** matrix differentiate between cutting states. The R-ratios have potential application in the control of orthogonal cutting.

2. EXPERIMENTAL APPARATUS

A schematic diagram of the experimental apparatus exployed is shown in Figure 1, and consists of a Hardinge CNC lathe, a special force dynamometer (utilizing three Kistler 9068 force transducers) and its associated electronics, and a digital spectrum analyzer (Hewlett Packard 3566A) for data acquisition and real-time analysis.

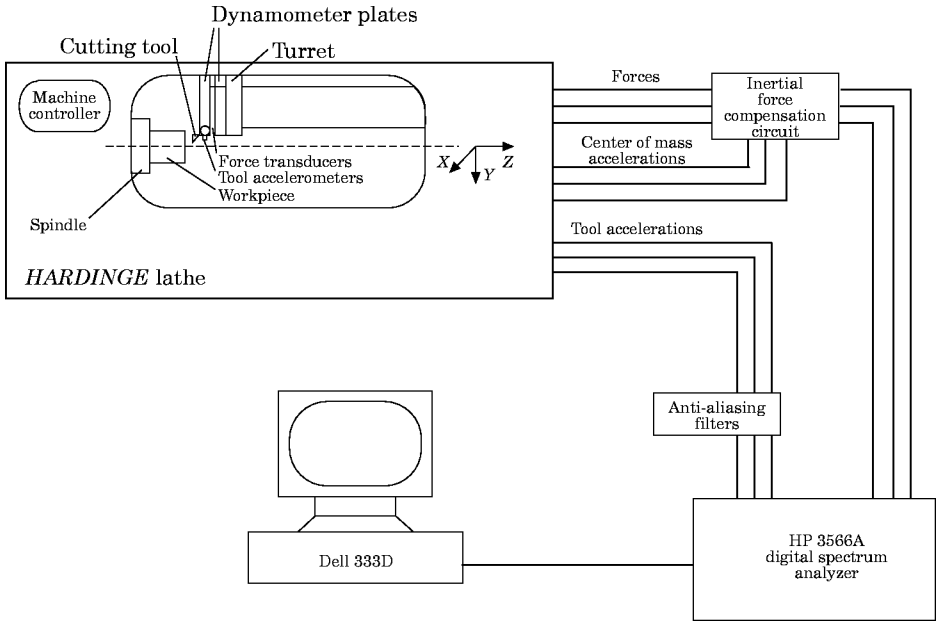

Figure 1. The experimental system.

All experiments involved only right-handed orthogonal cutting. Positive rake tool inserts were employed (Kennametal TPMR322) and were supported by Kennametal KT-GPR123B tool holders. The tool holder–insert combination resulted in a rake angle of 5° and a clearance angle of 4°. Cylindrical workpieces of 1020 steel were machined under a wide range of cutting conditions. Since all workpieces were stubby, workpiece modal characteristics did not affect the turning dynamics. The sampling rate was 4096 Hz and the cut off frequency was 1100 Hz. Averaging was performed over the time record assuming that, in each case, the system was in a steady state. Record lengths were from 20 to 60 s except for chatter records, which had a duration of 2 s.

3. THIRD ORDER RECURSION

The following definitions and theorems [16, 17] are included to provide a background in bispectral theory and for subsequent application. Let $c_3(\tau_1, \tau_2) \equiv$ the third order cumulant of the real third order stationary random process $X(k)$, $k = 0, \pm 1, \pm 2, \ldots$. If the mean of $X(k)$ vanishes, then $c_3(\tau_1, \tau_2) = m_3(\tau_1, \tau_2)$, where $m_3(\tau_1, \tau_2) = \mathrm{E}(X(k), X(k + \tau_1)X(k + \tau_2))$; E is the expected value, which may be estimated by

$$m_3(\tau_1, \tau_2) = (1/2n) \sum_{k=-n}^{+n} X(k)X(k + \tau_1)X(k + \tau_2), \tag{1}$$

where $n \to +\infty$. The bispectrum of $X(k)$, $C_3(\omega_1, \omega_2)$, is defined by

$$C_3(\omega_1, \omega_2) = \sum_{\tau_1=-\infty}^{+\infty} \sum_{\tau_2=-\infty}^{+\infty} c_3(\tau_1, \tau_2) \exp[-\mathrm{j}(\omega_1\tau_1 + \omega_1\tau_2)]; \tag{2}$$

$|C_3(\omega_1, \omega_2)| \equiv$ the bispectral index.

Consider an autoregressive, AR, estimation of the bispectrum, $C_3(\omega_1, \omega_2)$, equation (2) [16, 17]. A pth order AR process is described by

$$X(k) + \sum_{i=1}^{p} a(i)X(k-i) = W(k), \tag{3}$$

where it is assumed that $W(k)$ is non-Guassian, $\mathrm{E}(W(k)) = 0$, $\mathrm{E}(W^3(k)) = \beta$. Multiplying through equation (3), summing and noting equation (1) gives

$$c_3^x(-k, -l) + \sum_{i=1}^{p} a(i)c_3^x(i-k, i-l) = \beta\delta(k, l), \tag{4}$$

where $k, l > 0$. Letting $k = l$ in the third order recursion equation (4) with $k = 0, \ldots, p$ yields $p + 1$ equations for the $p + 1$ unknowns $a(i)$ and β; $p + 1 \equiv$ maxlag. In matrix notation,

$$\mathbf{Ra} = \mathbf{b}, \tag{5}$$

where

$$\mathbf{R} = \begin{vmatrix} g(0,0) & g(1,1) & \ldots g(p,p) \\ g(-1,-1) & g(0,0) & \ldots g(p-1,p-1) \\ \vdots & & \vdots \\ g(-p,-p) & g(-p+1,-p+1) & \ldots g(0,0) \end{vmatrix}, \tag{6}$$

$g(i, j) \equiv c_3^x(i, j)$, $\mathbf{a} \equiv [1, a(1), \ldots, a(p)]^{\mathrm{T}}$ and $\mathbf{b} \equiv [\beta, 0, \ldots, 0]^{\mathrm{T}}$. $\mathbf{R}$ is in general a non-symmetric Toeplitz matrix. A sufficient but not necessary condition for the representation in equation (5) to exist is the symmetry and positive definiteness of $\mathbf{R}$. A discussion of this and related conditions is given in reference [17]. The bispectrum corresponding to equation (3) is given by [4]

$$C_3^x(\omega_1, \omega_2) = \beta H(\omega_1)H(\omega_2)H^*(\omega_1 + \omega_2), \tag{7}$$

where

$$H(\omega) = 1 \Big/ \left(1 + \sum_{n=1}^{p} a(i) \exp(-\mathrm{j}\omega n)\right) \tag{8}$$

and $H^*(\omega) \equiv$ complex conjugate of $H(\omega)$.

An estimate of the $\mathbf{R}$ matrix, equation (6), and bispectrum, equation (7), for a data set $X(I)$, $I = 1, \ldots, N$, may be formed [16, 17] as follows.

(1) Segment the data set into K records of M samples each. $X^i(k)$, $k = 1, 2, \ldots, M$, are data points associated with the ith record.

(2) Compute $c_{3,i}^x(m, n)$ for the ith record as

$$c_{3,i}^x = (1/M) \sum_{l=a}^{b} X^{(i)}(l)X^{(i)}(l+m)X^{(i)}(l+n), \tag{9}$$

where $i = 1, 2, \ldots, K$, $a \equiv \max(1, 1-m, 1-n)$ and $b \equiv \min(M, M-m, M-n)$.

(3) Average $c^x_{3,i}(m, n)$ over all K records,

$$\hat{c}_3(m, n) = (1/K) \sum_{i=1}^{K} c^x_{3,i}(m, n), \tag{10}$$

to yield the estimate $\hat{c}_3(m, n)$ or $c_3(m, n)$. Form an estimated **R** matrix by replacing $c_3(m, n)$ by $\hat{c}_3(m, n)$ in equation (6). Estimated values of **a** follow from equation (5). These results implemented in reference [22] are subsequently applied to orthogonal cutting data.

AR models were shown in references [16, 17] to be effective detectors of quadratic phase coupling. Singular values of the **R** matrix, equation (6), of interest in the identification of orthogonal cutting states, are now considered.

4. SINGULAR VALUE DECOMPOSITION

Fundamental properties of singular values are discussed and applied to given phase coupled test functions. If **A** is a real $m \times n$ matrix, then there exist orthogonal matrices $\mathbf{U} \in \mathbf{R}^{m \times n}$ and $\mathbf{V} \in \mathbf{R}^{m \times n}$ such that

$$\mathbf{U}^{\mathrm{T}}\mathbf{A}\mathbf{V} = \mathrm{diag}(\sigma_1, \ldots, \sigma_q) \in \mathbf{R}^{m \times n}, \tag{11}$$

where $q = \min(m, n)$, $\sigma_1 \geqslant \sigma_2 \geqslant \ldots \geqslant \sigma_q \geqslant 0$ are the singular values and $\mathbf{R}^{m \times n}$ denotes a real $m \times n$ matrix. A criterion for selecting the autoregressive order, p, in equation (3) is given in references [17, 22]. p is chosen to equal the number of singular values of the **R** matrix which are above the noise floor. Note that if $\sigma_1 \geqslant \cdots > \sigma_r > \sigma_{r+1} = \cdots = \sigma_q = 0$, then rank $(\mathbf{A}) = r$; references [5, 7].

The singular values of the matrix **A** may be geometrically interpreted as the lengths of the semi-axes of the hyperellipsoid, E, defined by the mapping of the unit sphere $\mathbf{A}\mathbf{x}$, where **x** is an arbitrary unit vector, $|\mathbf{x}| = 1$. The singular values, σ_i, and their ratios are invariant with respect to translations and rigid rotations of E.

The singular values, $\sigma_i(\mathbf{A})$, and eigenvalues, $\lambda_i(\mathbf{A})$, of a square matrix, **A**, are closely related in several instances. If **A** is positive definite, then $\sigma_i(\mathbf{A}) = \lambda_i(\mathbf{A})$, while $\sigma_j(\mathbf{A}) = |\lambda_j(\mathbf{A})|$ if **A** is normal [5, 7]. A matrix $\mathbf{A} \in \mathbf{R}^{n \times n}$ is positive definite if $\mathbf{x}^{\mathrm{T}}\mathbf{A}\mathbf{x} > 0$ for all non-zero $\mathbf{x} \in \mathbf{R}^n$. A matrix $\mathbf{A} \in \mathbf{C}^{n \times n}$ is normal if $A^*A = AA^*$, where $\mathbf{A}^*$ is the Hermitian conjugate of **A**. It follows that **A** is normal if and only if there exists a unitary $\mathbf{Q} \in \mathbf{C}^{n \times n}$ such that $\mathbf{Q}^*\mathbf{A}\mathbf{Q} = \mathrm{diag}(\lambda_1, \ldots, \lambda_n)$; see references [5, 7]. Since **R** matrices, equation (6), associated with cutting data are neither positive definite nor normal, it follows that in general for these cases $\sigma_i(A) \neq |\lambda_i(A)|$.

Relationships between phase coupled trigonometric functions and the singular values of the corresponding **R** matrix were established through a study of three functions $f_i(t)$, where

$$f_1(t) = \cos(2\pi \times 100t + \phi_1) + \cos(2\pi \times 100t + \phi_2) + 0{\cdot}2\cos(2\pi \times 200t + \phi_1 + \phi_2), \tag{12}$$

$$f_2(t) = 0{\cdot}9\cos(2\pi \times 90t + \phi_1) + 1{\cdot}0\cos(2\pi \times 100t + \phi_2) + 0{\cdot}2\cos(2\pi \times 190t + \phi_1 + \phi_2), \tag{13}$$

$$f_3(t) = 1{\cdot}0\cos(2\pi \times 90t + \phi_1) + 1{\cdot}0\cos(2\pi \times 100t + \phi_2) + 1{\cdot}0\cos(2\pi \times 190t + \phi_1 + \phi_2) + 1{\cdot}0\cos(2\pi \times 100t + \phi_2) + 1{\cdot}0\cos(2\pi \times 110t + \phi_3) + 0{\cdot}5\cos(2\pi \times 210t + \phi_2 + \phi_3), \tag{14}$$

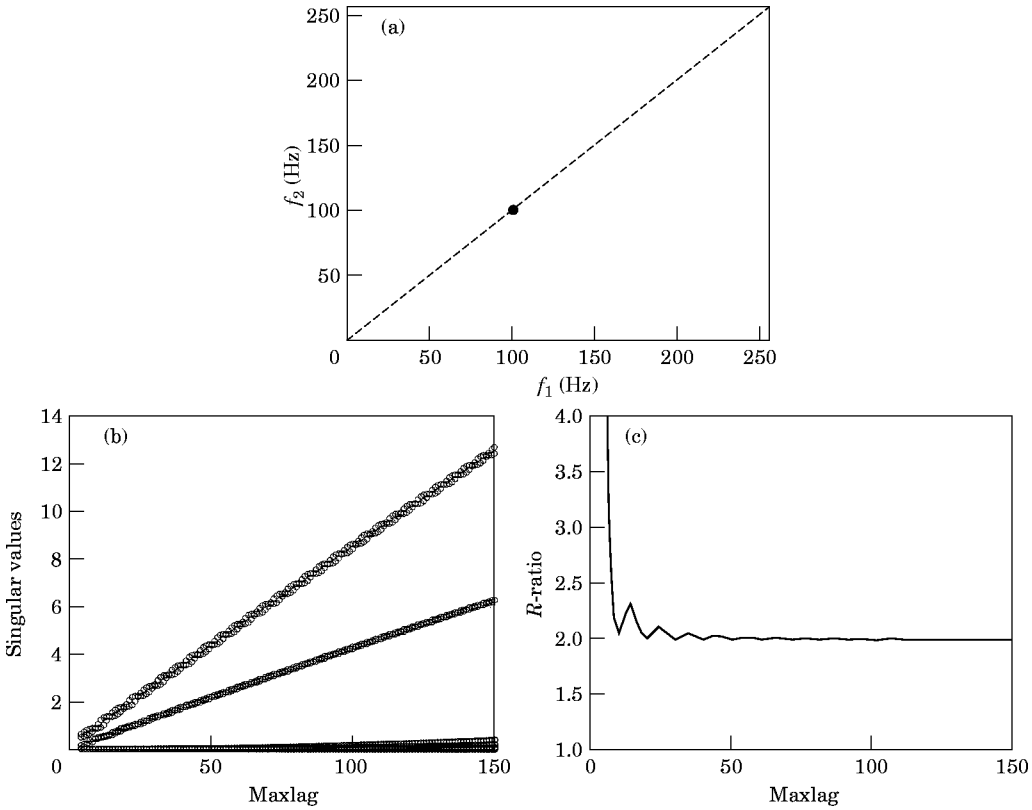

Figure 2. Test function $f_1(t)$; (a) Bispectrum of $f_1(t)$; (b) singular values versus maxlag for $f_1(t)$; (c) R-ratio versus maxlag for $f_1(t)$.

and where the ϕ_i are mutually independent and uniformly distributed over $[0, 2\pi]$. The $f_i(t)$ functions were sampled at 1024 Hz over an interval of 10 s. **R** matrices were evaluated for each $f_i(t)$ by averaging over ten 1 s intervals; see equations (6) and (9).

In equation (12), $f_1(t)$, is an example of the self-phase coupling of a 100 Hz frequency component. In the experimental data studied frequency components in the neighborhood of 100 and 200 Hz were always observed in the power spectra of cutting states close to chatter. A peak with frequency co-ordinates in the neighborhood of (100 Hz, 100 Hz), appeared in the bispectrum of cutting states in the neighborhood of chatter. The bispectrum, (2), of $f_1(t)$ is shown in Figure 2(a). A single peak is observed at (100, 100). The singular values of **R** are plotted in Figure 2(b) as a function of maxlag (4). A pair of singular values is associated with each frequency component. Singular values in the noise floor have no significance. The ratio of the mean of the largest pair of singular values to the mean of the second largest pair defines a non-dimensional ratio of invariants of **R**, the R-ratio. This ratio is shown as a function of maxlag for $f_1(t)$ in Figure 2(c): the R-ratio $\simeq 2{\cdot}0$ for maxlag > 30.

In equation (13), $f_2(t)$, involves the phase coupling of 90 and 100 Hz components. This approximates the coupling of the first natural frequency of the cutting system, $\simeq 100$ Hz, with a side band at 90 Hz. The bispectrum of $f_2(t)$ is shown in Figure 3(a). The peak at (100, 90) indicates phase coupling between the 90 and 100 Hz components. Symmetry of the bispectrum with respect to the line $f_1 = f_2$ results in a peak at (90, 100). The mean of

the first pair of singular values is nearly equal to the mean of the second pair of singular values for maxlag > 80. Note Figure 3(b) for maxlag > 90, for which $1{\cdot}0 < R\text{-ratio} \leqslant 1{\cdot}2$.

In equation (14), $f_3(t)$ is the sum of a phase coupled component at 100 Hz and 110 Hz and a phase coupling of 90 and 100 Hz components. The bispectrum of $f_3(t)$ is shown in Figure 4(a), with peaks at (100, 110), (100, 90) and (110, 100), (90, 100) because of symmetry. In Figure 4(b), the R-ratio is plotted as a function of maxlag, from which it is seen that the R-ratio $\simeq 1{\cdot}5$ for maxlag > 80.

In the instances discussed above, the R-ratio discriminates between the self-phase coupling of trigonometric functions, phase coupling of nearly equal frequency components and a linear combination of both. It is subsequently shown that f_1, f_2 and f_3 have R-ratios which share certain similarities with the R-ratios of near chatter states, heavy cutting, cutting states distant from chatter, light cutting and intermediate states.

5. CUTTING STATE CHARACTERIZATION

Sequences of cutting experiments were performed in which either the depth of cut or the turning frequency was varied with all other cutting parameters held constant. Singular values of **R**, equation (6), were computed for two sequences with variable turning frequency and five sequences with variable depth of cut over a turning frequency range of 290–852 rpm. Each variable cutting depth sequence ended in chatter while each variable

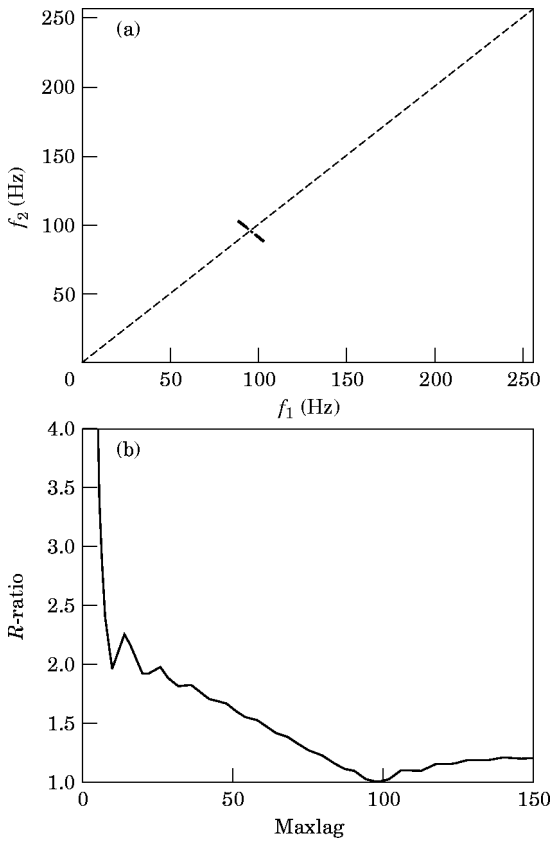

Figure 3. Test function $f_2(t)$. (a) Bispectrum of $f_2(t)$; (b) R-ratio versus maxlag for $f_2(t)$.

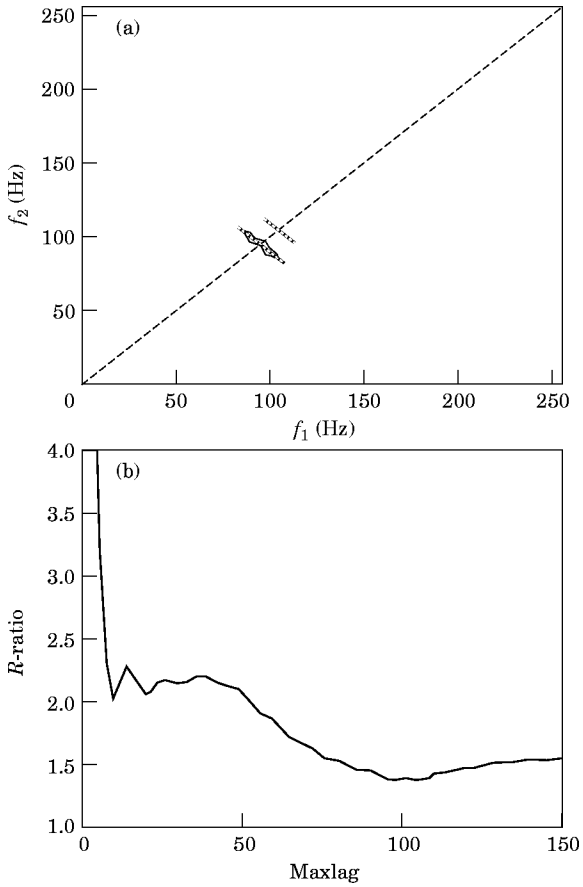

Figure 4. Test function $f_3(t)$. (a) Bispectrum of $f_3(t)$; (b) R-ratio versus maxlag for $f_3(t)$.

turning frequency sequence contained at least one chatter state. A total of 42 cutting experiments were performed. Typical sequences have been selected from the set.

For sequence 1, s-1, the following data was used: turning frequency = 460 rpm, rake angle = 5°, surface speed = 90 m/min, feed rate = 0·007 in/rev., re-sampling rate = 1024 Hz, frequency cut-off = 1100 Hz, and depth of cut = 2·5, 2·6, 2·7 and 2·8 mm, at which depth chatter was observed.

Singular values of **R**, equation (6), and the R-ratio versus maxlag are shown in Figures 5(a) and (b) for a depth cut of 2·5 mm which corresponds to light cutting. Four dominant singular values occur in two pairs, which approach each other as the parameter maxlag increases. The R-ratio, shown in Figure 5(b), is close to 1·0. For $70 \leqslant \text{maxlag} \leqslant 100$, $1{\cdot}12 \geqslant R \geqslant 1{\cdot}08$. The behavior of the R-ratio as a function of maxlag has similarities with that of $f_2(t)$, in equation (13); see Figure 3(b). $f_2(t)$ contains two phase coupled trigonometric functions of 90 and 100 Hz which approximate phase coupling between the first natural frequency of the system at 98 Hz and a lower frequency component of the sideband structure.

Chatter was observed for a depth cut of 2·8 mm. Singular values of **R** and the R-ratio versus maxlag are shown in Figures 6(a) and (b). One pair of singular values is dominant. For $20 \leqslant \text{maxlag} \leqslant 100$, $2{\cdot}0 \leqslant R\text{-ratio} \leqslant 2{\cdot}4$. The R-ratio as a function of maxlag is similar to that of $f_1(t)$, in equation (12)—see Figures 2(b) and 6(b)—which represents

self-phase coupling of the 100 Hz component. The presence of self-phase coupling in the time series is confirmed by peaks in the power spectrum at 100 and 200 Hz and a peak in the bicoherence index at (100, 100). These results are consistent across all sequences of experiments in which the depth of cut varies. For increasing depth of cut the R-ratio clearly differentiates between light cutting and chatter.

Two intermediate states with depths of cut of 2·6 and 2·7 mm complete the sequence s-1. Singular values and the R-ratio versus maxlag are shown in Figures 7(a) and (b), respectively, for the 2·6 mm case. For $50 \leqslant \text{maxlag} \leqslant 110$, the R-ratio $\simeq 1{\cdot}6$; see Figure 7(b). There is a similarity between Figure 4(b), the R-ratio for $f_3(t)$, and Figure 7(b). The R-ratios are close to one another for $50 \leqslant \text{maxlag} \leqslant 110$.

Singular values and the R-ratio versus maxlag are shown in Figures 8(a) and (b), respectively, for the 2·7 mm case. For maxlag > 60 the R-ratio $< 2{\cdot}0$ declines to 1·35 for maxlag $= 150$, Figure 8(b). The largest pair of singular values, shown in Figure 8(a), behaves similarly to the largest pair of the chatter case, shown in Figure 6(a), for maxlag < 60. For maxlag > 60 the previous smaller pair of singular values is replaced by a pair with a trajectory of greater slope, being nearly parallel with the trajectory of the

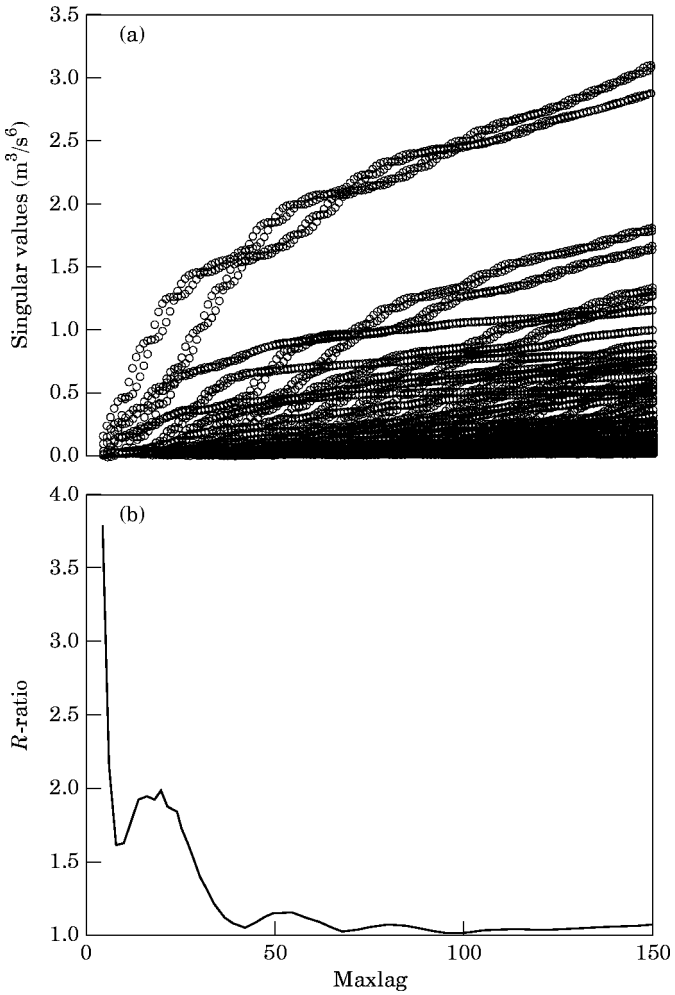

Figure 5. Data set s-1, 2·5 mm. (a) Singular values versus maxlag; (b) R-ratio versus maxlag.

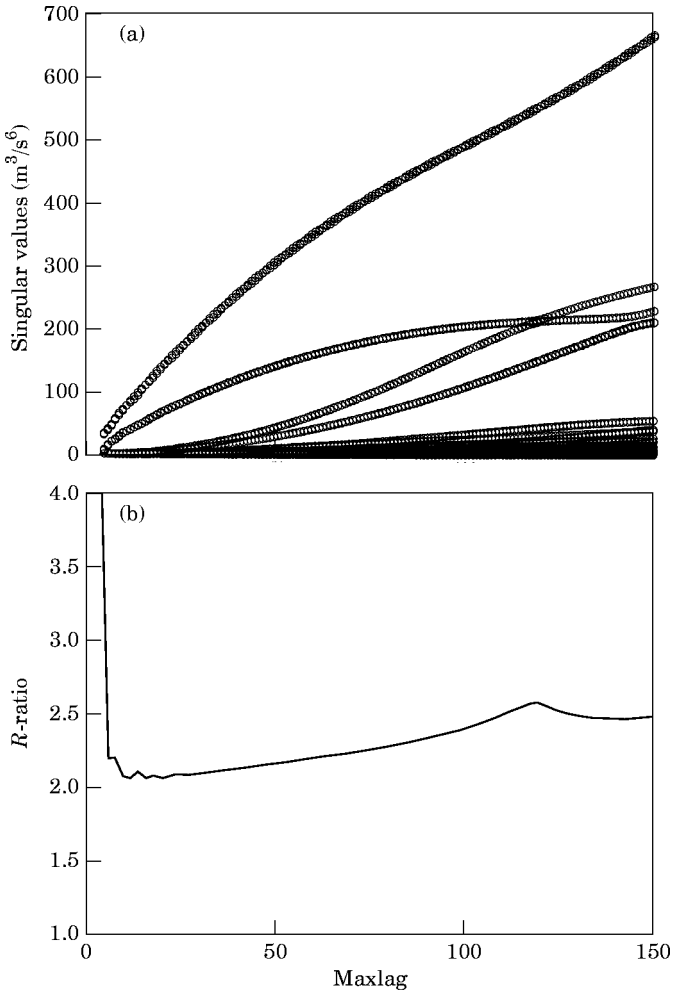

Figure 6. Data set s-1, 2·8 mm. (a) Singular values versus maxlag; (b) *R*-ratio versus maxlag.

largest pair. The distance between the pairs remains constant; consequently their ratio decreases as their magnitude increases. The f_i test functions do not exhibit this behavior; see equations (12), (13) and (14).

Sequence 2, s-2, is characterized as follows: depth of cut = 2·8 mm, rake angle = 5°, surface speed = 90 m/min, feed rate = 0·007 in/rev, re-sampling rate = 1024 Hz, frequency cut-off = 1100 Hz, and turning frequency = 335, 360, 371, 380 and 390 rpm. Chatter was observed at 371 rpm. The boundary between the chatter and non-chatter states consists of a series of lobes which, as a function of cutting depth, project downward into the non-chatter region. In contrast to s-1, this results in the occurrence of multiple chatter states as a function of the experimental variable turning frequency. The choice of depth of cut = 2·8 mm places many of the experimental cutting states close to, if not in the chatter region. The 360–390 rpm cases are spaced at roughly 10 rpm intervals, symmetrically situated with respect to the chatter state at 371 rpm. The *R*-ratio for the chatter state, shown in Figure 9(a), bears a strong resemblance to the *R*-ratio of the chatter state occurring in s-1; see Figure 6(b). In Figure 9(a), $2{\cdot}0 \leqslant R\text{-ratio} \leqslant 2{\cdot}3$ for $12 \leqslant \text{maxlag} \leqslant 150$.

The R-ratios for s-2, 360 and 380 rpm, are given in Figures 9(b) and (c), respectively. Their qualitative behavior is similar to that of the cutting state shown for s-1, 2·7 mm—see Figure 8(b)—which immediately precedes the chatter state at s-1, 2·8 mm; see Figure 6(b). In Figures 9(b) and (c) is shown a maximum in the R-ratio of approximately 2·5 in the neighborhood of maxlag = 60. The R-ratio for s-2, 360 and 380 rpm decreases for maxlag > 60, reaching values of 1·99 and 1·68 at maxlag = 100 and 1·5 and 1·3 at maxlag = 150, respectively. The R-ratio for s-2, 390 rpm, is differentiated from the previous two cases, reaching a maximum value of 2·5 at maxlag = 40 and decreases to 1·07 at maxlag = 100; see Figure 9(d). The R-ratio versus maxlag plot for s-2, 335 rpm, shown in Figure 9(e), is similar to the plots of s-2, 360 and 390 rpm.

The time series studied are modulated by a function with a fundamental frequency equal to the turning frequency. The peak in the R-ratio versus the maxlag plots for s-2, 335, 360 and 380 rpm, occur at maxlag $\simeq$ 65. This corresponds to one half of the period of the fundamental frequency of the modulation function. The decline in the R-ratio for maxlag > 65 may therefore be caused by the detection of the modulation function.

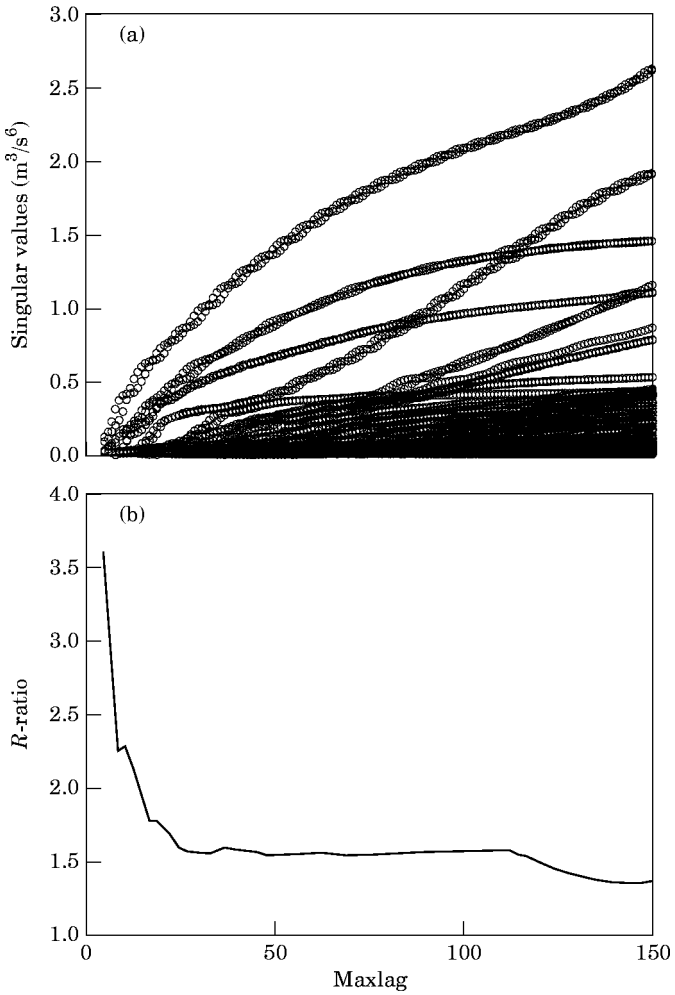

Figure 7. Data set s-1, 2·6 mm. (a) Singular values versus maxlag; (b) R-ratio versus maxlag.

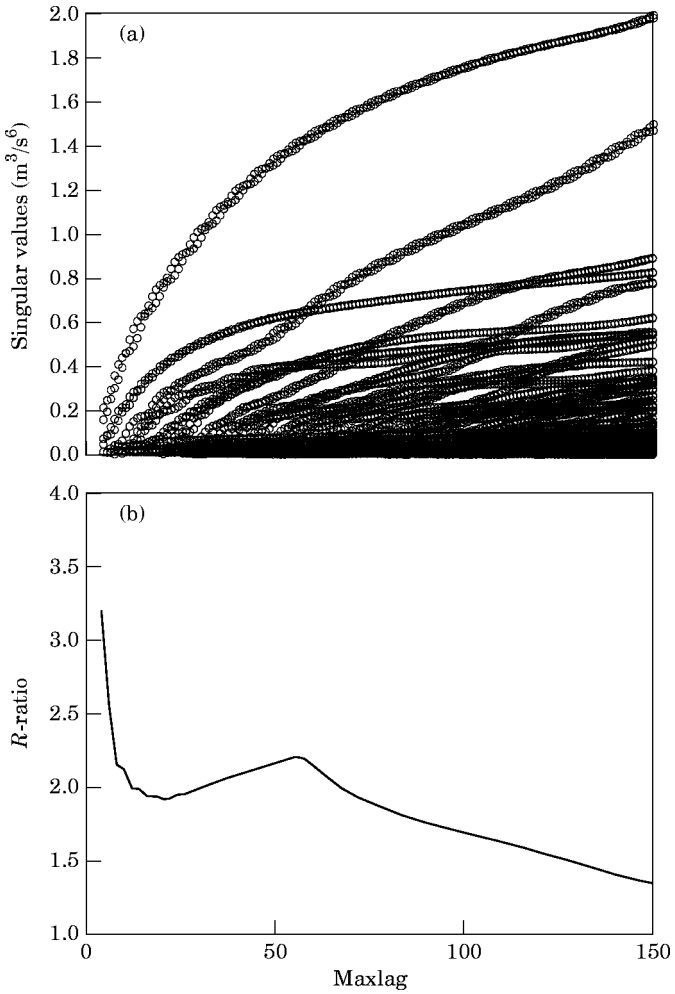

Figure 8. Data set s-1, 2·7 mm. (a) Singular values versus maxlag; (b) *R*-ratio versus maxlag.

6. CONCLUSIONS

The presence of quadratic phase coupling in orthogonal cutting time series has been previously demonstrated [3]. The Toeplitz **R** matrix, given in equation (6), of the third order cumulants was shown in references [16, 17] to determine the coefficients in an autoregressive esimation of the bispectrum. In the present study singular values of **R**, based on cutting tool acceleration measurements, were shown to characterize cutting states, differentiating between light cutting, pre-chatter and chatter. In particular, the ratio of the mean of the two dominant pairs of singular values, the *R*-ratio, evaluated for maxlag = 100, approximates one for light cutting, two or more for chatter and near chatter states and takes intermediate values for intermediate states, increasing from one to two as chatter is approached. This behavior was observed in an analysis of tool acceleration time series for five sequences of cutting experiments with increasing depth of cut and two sequences with variable turning frequency. All experiments utilized very stiff workpieces, with the tool geometry and material properties held constant. For chatter and light and intermediate cutting the *R*-ratio is seen to be a constant or slowly changing function of

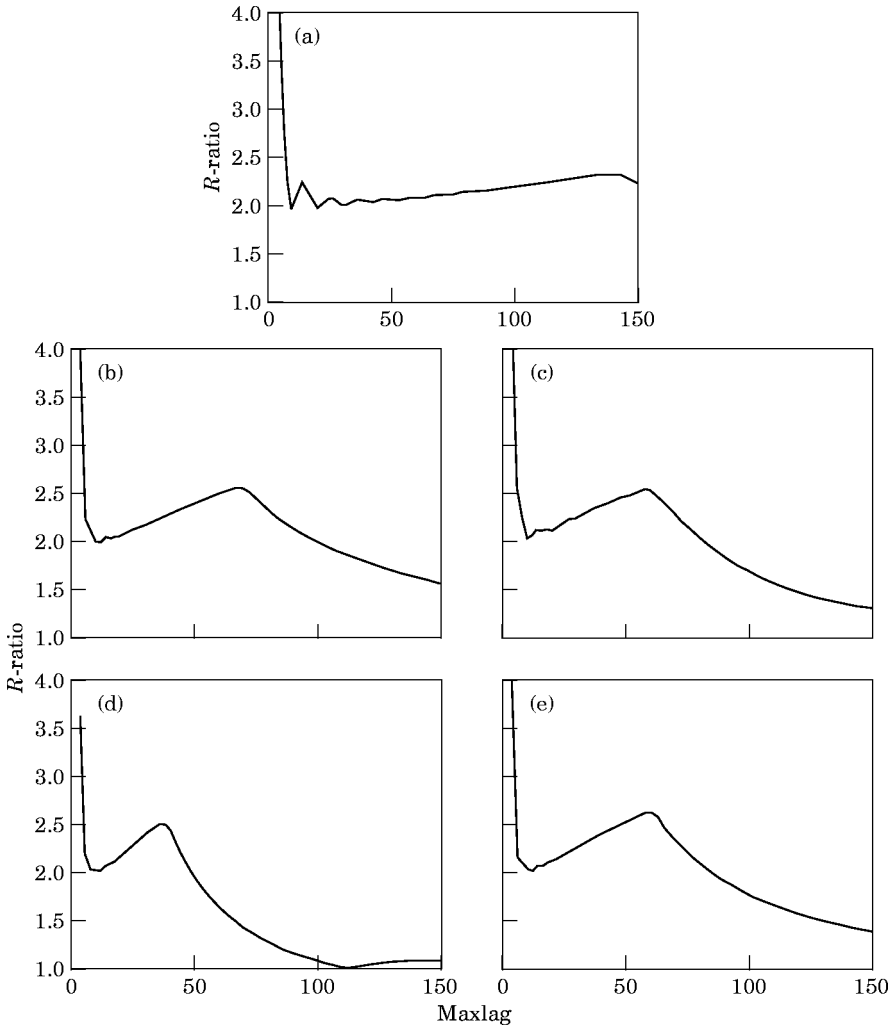

Figure 9. Data set s-1; R-ratio versus maxlag. (a) 371 Hz; (b) 360 Hz; (c) 380 Hz; (d) 390 Hz; (e) 335 Hz.

maxlag for maxlag > 40, as given in equation (4); see Figures 5(b), 6(b), 7(b) and 9(a). The R-ratio versus maxlag function for near chatter cutting states exhibited a well defined maximum in the interval $40 <$ maxlag < 65, followed by a relatively steep decline; see Figures 8(b) and 9(b)–(e). In some instances, the R-ratio appeared to approach an asymptotic limit for maxlag > 100.

The application of neural networks to chatter identification in reference [23] required the characterization of chatter by other means, so that training functions could be constructed with the necessary characteristic properties. For the experimental data examined here, the R-ratio characterized a continuous range of cutting states from light cutting to chatter without the necessity of training procedures. However, once trained, neural nets were shown to be capable of on-line chatter identification.

In the wavelet analysis of reference [8] the identification of cutting states was based on qualitative features of wavelet based time–frequency plots. The R-ratio provides a qualitative, and evaluated for a specific value of maxlag, a quantative characterization of

the cutting state. Test functions were studied with R-ratios versus maxlag, as given in equation (4), plots similar to those of the cutting states. The R-ratio and other non-dimensional functions of singular values find application in the control of orthogonal cutting.

ACKNOWLEDGMENTS

The authors acknowledge the support of the D.O.E. through DE-FG02-93ER14335 and the N.S.F. through GER-9354956. The encouragement of O. Manley, of the D.O.E., and of P. Grootenhuis and D. J. Ewins, of Imperial College of Science and Technology, London, is appreciated.

REFERENCES

1. H. D. I. Abarbanel, R. Brown, J. J. Sidorowich and L. S. Tsimring 1993 *Reviews of Modern Physics* **65**(4), 1331–1392. The analysis of observed chaotic data in physical systems.
2. T. Y. Ahn, K. F. Eman and S. M. Wu 1985 *Transaction of the American Society of Mechanical Engineers*, *Journal of Engineering for Industry* **107**, 91–94. Cutting dynamics identification by dynamic data system modeling approach.
3. B. S. Berger, I. Minis, K. Deng, Y. S. Chen, A. Chavali and M. Rokni 1996 *Journal of Sound and Vibration* **191**, 986–992. Phase coupling in orthogonal cutting.
4. D. R. Brillinger and M. Rosenblatt 1967 in *Spectral Analysis of Time Series* (B. Harris, editor). New York: John Wiley. Asymptotic theory of kth order spectra. Also: *idem* 1967 in *Spectral Analysis of Time Series* (B. Harris, editor). New York: John Wiley. Computation and interpretation of kth order spectra.
5. G. H. Golub and C. F. Van Loan 1993 *Matrix Computations*. Baltimore, MD: The Johns Hopkins University Press.
6. R. M. Gray 1972 *IEEE Transactions on Information Theory* **IT-18**(6), 725–730. On the asymptotic eigenvalue distribution of Toeplitz matrices.
7. R. A. Horn and C. R. Johnson 1991 *Topics in Matrix Analysis*. Cambridge: Cambridge University Press.
8. M. K. Khraishen, C. Pezeshki and A. E. Bayoumi 1995 *Journal of Sound and Vibration* **180**, 67–87. Time series based analysis for primary chatter in metal cutting.
9. K. J. Kim, E. F. Eman and S. M. Wu 1984 *International Journal of Machine Tool Design and Research* **27**, 161–170. Identification of natural frequencies and damping ratios of machine tool structures by the dynamic data system approach.
10. I. Koenigsberger and J. Tlusty 1971 *Structure of Machine Tools*. New York: Pergamon Press.
11. M. Kronenberg 1966 *Machining Science and Application*. New York: Pergamon Press.
12. J. S. Lin and C. I. Weng 1990 *International Journal of Machine Tools and Manufacturing* **30**, 53–64. A nonlinear model of cutting.
13. J. M. Mendel 1990 *SPIE Advanced Signal-Processing Algorithms*, *Architectures and Implementations* **1348**, 20–25. Higher-order statistics and their application in signal processing.
14. M. E. Merchant 1945 *Journal of Applied Physics* **16**, 267–275. Mechanics of metal cutting process I.
15. I. Minis, B. S. Berger, V. A. Chavali and Y. H. Chen 1995 Experimental analysis of time series in machining dynamics, submitted for publication.
16. C. L. Nikias and J. M. Mendel 1993 *IEEE Signal Processing Magazine* July, 10–37. Signal processing with higher-order spectra.
17. C. L. Nikias and A. P. Petropulu 1993 *Higher-order Spectra Analysis*. Englewood Cliffs, NJ: Prentice Hall.
18. J. Peters, P. Vanderck and H. Van Brussel 1971 *CIRP Annals* **20**, 129–136. The measurement of the dynamic cutting coefficient.
19. M. Weck 1985 *Handbook of Machine Tools*, Volume 4. New York: John Wiley.
20. M. R. Raghuveer and C. L. Nikias 1985 *IEEE Transactions on Acoustics*, *Speech and Signal Processing* **ASSP-33**(4), 1213–1230. Bispectrum estimation: a parametric approach.
21. A. Ruhe 1975 *Linear Algebra and its Applications* **11**, 87–94. On the closeness of eigenvalues and singular values for almost normal matrices.

22. A. Swami, J. M. Mendel and C. L. Nikias 1993 *Hi Spec Toolbox*. Matick, MA: Math Works, Inc.
23. I. N. Tansel, A. Wagiman and T. Tziranir 1991 *International Journal of Machine Tools and Manufacturing* **31**(4), 539–552. Recognition of chatter with neural networks.
24. H. R. Taylor 1977 *Proceedings of the Institute of Mechanical Engineers* **191**, 257–270. A comparison of methods for measuring the frequency response of mechanical structures with particular reference to machine tools.
25. J. Tlusty 1979 *CIRP Annals* **27**, 583–589. Analysis of the state of research in cutting dynamics.
26. D. W. Wu and C. R. Liu 1985 *Transactions of the American Society of Mechanical Engineers*, *Journal of Engineering for Industry* **107**, 107–118. An analytical model of cutting dynamics, parts 1 and 2.
27. D. W. Wu 1989 *Transactions of the American Society of Mechanical Engineers*, *Journal of Engineering for Industry* **11**, 37–47. A new approach to formulating the transfer function for dynamic cutting processes.